Geometric evolution law for modeling strongly anisotropic thin-film morphology

Christopher Ograin*
University of California, Santa Barbara, California 93106, USA

John Lowengrub†
University of California, Irvine, California 92697, USA
(Received 24 August 2011; published 20 December 2011)

The morphology of the solid-vapor interface of a nanoscale thin crystalline film is influenced by many factors including surface diffusion, attachment-detachment, deposition, and interface kinetics. Using a high-order accurate and efficient numerical method, we investigate the dynamics of two dimensional thin films when all of these effects are considered. The observed morphologies consist of facets of constant slope separated by narrow transition intervals: kinks (valleys) and antikinks (hills). The number of kinks and antikinks decreases as the system coarsens in time. Our numerical results confirm that when deposition is present, the only possible coarsening event is the kink-ternary where two kinks meet and annihilate an antikink. We characterize the total amount of coarsening, the time over which the coarsening occurs and the associated coarsening scaling laws when all effects are considered. As found in previous work that considered only attachment-detachment, or surface diffusion, there are three distinct coarsening regimes associated with increasing magnitudes of the deposition flux—fast coarsening, a regime in which periodic structures form with little or no subsequent coarsening, and a regime in which the film surface evolves chaotically. We find that the inclusion of attachment-detachment leads to additional coarsening compared to the dynamics that result from driven surface diffusion alone. When deposition and interface kinetics are both considered, the slowdown of evolution caused by the kinetic effects necessitates a decrease in the deposition flux in order to produce a nonchaotic coarsening regime. Together, these provide testable predictions for experiments of thin-film dynamics.

DOI: 10.1103/PhysRevE.84.061606 PACS number(s): 81.10.Aj, 05.70.Np, 05.45.−a, 68.55.−a

I. INTRODUCTION

The problem of understanding the evolution of nanoscale thin films is of great interest to researchers in a variety of fields in materials science. A model problem consists of the deposition of a metallic alloy vapor on a metallic substrate. The evolution of the interface may show a variety of different types of structures depending on the temperature and deposition rate. For example, studies show the formation of dislocation-free islands, which coarsen with time [1,2]. The self-assembly of such structures at the nanoscale is seen as a means to efficiently produce novel nanoscale components of advanced electronic and optoelectronic devices.

For over a century researchers have been attempting to characterize the behavior of crystalline surfaces (e.g., [3]). In 1901, Wulff [4] introduced a construction for the equilibrium shape of an interface. The so-called "Wulff shape" of a crystal in two dimensions is the shape of minimum surface free energy under the constraint of fixed area. In 1951, Burton, Cabrera, and Frank [5] developed a tangent angle formulation and gave a specific parametrization of the Wulff shape. When the anisotropy is strong, there are missing orientations in the Wulff shape and sharp corners develop. The corresponding evolution problem (gradient flow) becomes ill-posed. To regularize this problem, DiCarlo, Gurtin, and Podio-Guidugli [6] added a bending or Willmore energy to the system. In particular, the additional energy term is proportional to the square of the mean curvature of the interface. Spencer [7] showed that solutions to the regularized model approach the Wulff shape as the regularization constant approaches zero. Here we will use the Willmore regularization approach. We note that other regularization methods may be performed, such as the convexification technique considered by Eggleston *et al.* [8].

The regularization of ill-posed models for faceted crystals is not the only approach to modeling the crystal morphologies, however. Another approach involves appealing to microscopic processes and incorporating the dynamics of atomic steps. For example, in Ref. [9], such an approach was used to study the morphological equilibration of a faceted crystal when surface diffusion is the main transport mechanism but kink attachment-detachment, edge transfer and terrace hopping are also considered. Other results using atomic step dynamic approaches can be found in Refs. [10–13].

We study interface evolution in two dimensions in which the morphology is driven by surface diffusion, attachment-detachment (motion-by-curvature), deposition, and kinetic effects. These factors have been studied individually in a full geometric setting as well as in a long-wave approximation. However, until now, no study has considered the combined effects of all of these processes.

In the case of driven anisotropic motion by curvature, Watson [14] drew a connection between the geometric equation and a convective Cahn-Hilliard (cCH) equation and showed that the cCH equation is the long-wave approximation for driven anisotropic motion by curvature. Watson *et al.* [15] performed a matched asymptotic analysis of the cCH equation and established a theory for coarsening in the resulting dynamical system. In particular it was shown both numerically and analytically that the kink-ternary behavior, in which two kinks come together to annihilate an antikink, is the only possible

*ograin@math.ucsb.edu
†lowengrb@math.uci.edu

coarsening event for evolution governed by the cCH equation. Recent analytical work by Watson [16] demonstrates that an identical result holds for the full geometric equation. Spinodal decomposition and coarsening of thermodynamically unstable crystal surfaces under the influence of strong anisotropic (nonconvex) surface free energy densities and driven by surface diffusion has been considered in [17–19]. However, all of these theoretical and numerical treatments are restricted to linear stability analyses and long-wave approximations based on small variations in surface orientation. For example, Savina *et al.* [19] performed an analysis of a higher-order cCH equation, which represents the long-wave approximation associated with driven anisotropic surface diffusion.

Haußer and Voigt [20] performed numerical simulations for the full geometric equation for driven anisotropic motion by curvature. Their results show the same kink-ternary behavior as that seen for the cCH equation. Also, they identify three different coarsening regimes which depend on the rate of deposition: fast coarsening, a regime in which periodic structures form, and a regime in which chaotic evolution occurs. These regimes are distinguished by the driving force constant—the rate of deposition. The identification of these regimes is similar to those found by Golovin *et al.* [21] for the cCH equation, which is associated with attachment-detachment but not surface diffusion. In the context of surface diffusion, Savina *et al.* [19] demonstrated that these coarsening regimes also occur in a higher-order cCH approximation to driven anisotropic surface diffusion. Haußer and Voigt found these different coarsening regimes numerically in the full geometric setting for surface diffusion (see Fig. 16 in [22]).

Stöcker and Voigt [23] studied the inclusion of kinetic effects on the surface diffusion model to account for the rearrangement of particles on the interface. They used a numerical method based on a level set–finite-element formulation of the problem. They compared results obtained when surface diffusion is considered alone and those obtained by considering surface diffusion with a kinetic component. They find that the inclusion of a kinetic component serves to slow down the dynamics of the interface. They did not consider deposition or attachment-detachment and they did not analyze coarsening rates and scaling.

Here, we investigate numerically the combined effects of deposition, attachment-detachment, and interface kinetics using a high-order accurate and efficient numerical method. We characterize the total amount of coarsening, the time over which the coarsening occurs, and the associated coarsening scaling laws. The outline of the remainder of the paper is as follows. In Sec. II the model is introduced and nondimensionalized. In Sec. III, the numerical methods are presented. Results are shown in Sec. IV and finally conclusions are given in Sec. V where future directions are also discussed. In the Appendix V, we show analytically the relationship between the full geometric model used here and a long-wave approximation such as that developed in Ref. [19] for driven surface diffusion.

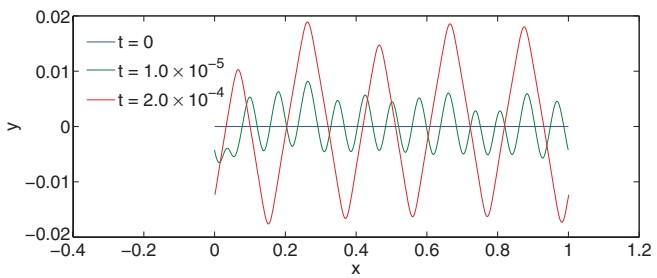

FIG. 1. (Color online) Interface evolution with $k = b = 0$, $\epsilon = 5.0 \times 10^{-3}$, and $c = 8.0 \times 10^{4}$.

II. A GEOMETRIC EVOLUTION MODEL

We consider the evolution of a one-dimensional periodic interface Γ, whose surface free energy is given by

$$E = E_0 \int_\Gamma \left(\tau(\theta) + \frac{\epsilon^2}{2}\kappa^2 \right) ds, \tag{1}$$

where E_0 is a constant of dimension energy per length. We also have that τ is a dimensionless anisotropy function depending on the local tangent angle θ, and s is the arc length along the interface. The second term in the integrand is a regularizing term in which κ denotes the curvature and ϵ is a constant of dimension length associated with the regularization. In two spatial dimensions, identifying $\kappa = \theta_s$, this energy can be thought of as a Cahn-Hilliard type energy with the anisotropic surface energy playing the role of the potential. The variational derivative of E with respect to variations in Γ is given by

$$\frac{\delta E}{\delta \Gamma} = E_0 \left[\tilde{\tau}(\theta)\kappa - \epsilon^2 \left(\kappa_{ss} + \frac{\kappa^3}{2} \right) \right], \tag{2}$$

where $\tilde{\tau}(\theta) = \tau''(\theta) + \tau(\theta)$ is the interface stiffness. When the surface energy is strongly anisotropic, there may be orientations for which the value of the stiffness function is negative. The resulting equations are ill-posed when $\epsilon = 0$. In the equilibrium shape orientations are missing, and sharp corners may form due to missing orientations. The regularizing term serves to penalize the formation of sharp corners when the anisotropy is sufficiently strong. This idea seems to have been introduced in Ref. [24] in two dimensions and in Ref. [6] in three dimensions. It was shown in Ref. [7] that the regularized solution approaches the classical equilibrium solution at a sharp corner as the regularization constant ϵ tends to zero. Also, a linear stability analysis similar to that found in Ref. [15] shows that the facets are constant to leading order. This suggests that at least for small ϵ, the regularization has a negligible effect at the facets.

We consider an interface evolution given by the system of equations

$$\rho V = (\nu \mu_s)_s - k\mu + c, \tag{3}$$

$$bV = \frac{\delta E}{\delta \Gamma} + \rho\mu, \tag{4}$$

where V represents the normal velocity of the interface, ρ is the density of the solid with dimensions mass per area, μ is the chemical potential in the solid with dimensions energy per mass, and c is a positive constant driving force representing deposition onto the interface with dimensions mass per length-time. The parameter ν is a non-negative coefficient corresponding to surface diffusivity with dimensions mass-time per length, k is a non-negative coefficient for attachment-detachment with dimensions mass-time per length^3, and b is a

non-negative coefficient associated with kinetic effects having dimensions mass per length-time. This model is derived on the basis of thermodynamic consistency and mass conservation; see, for example, Refs. [10,22,23,25,26]. Now we rescale the equation with respect to the length scale l and intrinsic time scale $\rho^2 l^4/\nu E_0$,

$$s = l\bar{s}, \tag{5}$$

$$t = \frac{\rho^2 l^4}{\nu E_0}\bar{t}, \tag{6}$$

where the bars denote dimensionless quantities. Then Eqs. (3) and (4) become

$$(1+\bar{k}\bar{b})\bar{V} - \bar{b}\bar{V}_{\bar{s}\bar{s}} = -\left[\overline{\frac{\delta E}{\delta\Gamma}}\right]_{\bar{s}\bar{s}} + \bar{k}\overline{\frac{\delta E}{\delta\Gamma}} + \bar{c}, \tag{7}$$

where

$$\bar{V} = \frac{\rho^2 l^3 V}{\nu E_0}, \tag{8}$$

$$\bar{k} = \frac{l^2 k}{\nu}, \tag{9}$$

$$\bar{b} = \frac{\nu b}{\rho^2 l^2}, \tag{10}$$

$$\bar{c} = \frac{\rho l^3 c}{\nu E_0}, \tag{11}$$

$$\bar{\epsilon} = \frac{\epsilon}{l}, \tag{12}$$

$$\overline{\frac{\delta E}{\delta\Gamma}} = \tilde{\tau}(\theta)\kappa - \bar{\epsilon}^2\left(\kappa_{\bar{s}\bar{s}} - \frac{\kappa^3}{2}\right). \tag{13}$$

Dropping the bar notation, we rewrite Eq. (7) in a frame of reference comoving with the planar front $\theta = 0$, with velocity $V = \frac{c}{1+kb}$. The resulting evolution equation is

$$(1+kb)V - bV_{ss} = -\left[\frac{\delta E}{\delta\Gamma} - \frac{bc}{1+kb}\cos\theta\right]_{ss} + k\frac{\delta E}{\delta\Gamma} + c(1-\cos\theta). \tag{14}$$

We use a typical anisotropy function of the form

$$\tau(\theta) = 1 + a\cos 4\theta, \tag{15}$$

which leads to the stiffness function

$$\tilde{\tau}(\theta) = 1 - 15a\cos 4\theta. \tag{16}$$

In our simulations we use $a = 0.1$. If $a > \frac{1}{15}$, then the stiffness function is negative for certain orientations. Thus the particular value of a that we have chosen necessitates the use of the regularization. We set the regularization parameter to be $\epsilon = 0.005$.

We study the evolution of a perturbed, nearly flat interface. Numerical results indicate an initial stage in which rapidly growing hills and valleys emerge; see Fig. 1. The numerical method is described later in Sec. III. A linear stability analysis of Eq. (7) provides a prediction for the maximum unstable mode, which in the case $k = b = 0$ is found to be given by $j = \sqrt{15a-1}/(\sqrt{6}\,\pi\epsilon)$. With our chosen parameters $a = 0.1$ and $\epsilon = 0.005$, we find that $j = 100/(\sqrt{3}\,\pi) \approx 18.38$. Indeed, as seen in Fig. 1, the wave number of the hill-valley structure in the early stages of interface evolution is about 18.

As evolution of the interface continues, we find facets with nearly constant slope, $\beta \approx \pm 0.38$, the energetically favored slope predicted by the Wulff shape; see Fig. 2 (lower). We note that the slopes of the facets are nearly constant, but not entirely. This variation of facet slopes is consistent with other findings [14,19] and is not an effect of the numerics. As mentioned earlier, a linear stability analysis similarly shows that the facets are constant to leading order. However, at the next order, there is some variation, which causes this small deviation from constant slope. The facets are separated by narrow transition intervals of length scale proportional to ϵ. These transition intervals are the hills (antikinks) and valleys (kinks) of the resulting interface shape; see Fig. 2. For positive values of the driving force constant c, the dynamics at later times exhibits coarsening events in which the kinks and antikinks annihilate each other until an equilibrium is reached. It is observed that the only type of coalescence event is the meeting of two kinks annihilating an antikink, known as the kink-ternary process. This coarsening behavior has been observed previously for the cCH equation [15] and the full geometric equations for driven anisotropic motion by curvature [20] and driven anisotropic surface diffusion [22]. Recent analytical work by Watson [16] shows that the kink-ternary process is the only possible coarsening event for the full geometric equation governing driven anisotropic motion by curvature. As we demonstrate later, larger values of the driving force constant produce a chaotic evolution for which there is no equilibrium.

III. NUMERICAL METHOD

Our numerical method is adapted from Ref. [27]. The idea is to consider an open plane curve Γ, given by $\mathbf{X}(\alpha,t) = (x(\alpha,t), y(\alpha,t))$, where α parametrizes the curve. We require that $x = \alpha + p(\alpha,t)$ and $y = q(\alpha,t)$ with p and q are one-periodic in α. The evolution of the curve is formulated as

$$s_{\alpha t} = T_\alpha - \theta_\alpha V, \tag{17}$$

$$\theta_t = \frac{T}{s_\alpha}\theta_\alpha + \frac{1}{s_\alpha}V_\alpha, \tag{18}$$

where s is the arc length, θ is the tangent angle, V is the normal velocity, and T is the tangential velocity of the interface. Following [27], we require that $s_\alpha = P(t)$ where P is the length of Γ. This leads to the system of equations

$$T(\alpha,t) = T(0,t) - \int_0^\alpha \theta_{\bar{\alpha}} V\, d\bar{\alpha} + \alpha\int_0^1 \theta_{\bar{\alpha}} V\, d\bar{\alpha}, \tag{19}$$

$$P'(t) = -\int_0^1 \theta_{\bar{\alpha}} V\, d\bar{\alpha}, \tag{20}$$

$$\theta_t = \frac{1}{P}(\theta_\alpha T + V_\alpha), \tag{21}$$

from which we can calculate $P(t)$ and $\theta(\alpha,t)$. The specific choice for the tangential velocity given by Eq. (19) guarantees that the grid points are equally spaced in arclength. This set of equations is enough to give the complete evolution of Γ. The coordinates of the interface are recovered by integrating

$$x_\alpha = P\cos\theta \quad \text{and} \quad y_\alpha = P\sin\theta. \tag{22}$$

To calculate P we use the second-order Adams-Bashforth method,

$$P^{n+1} = P^n + \frac{\Delta t}{2}(3M^n - M^{n-1}), \tag{23}$$

where M is given by

$$M = -\int_0^1 \theta_{\alpha'} V d\alpha', \tag{24}$$

and V is taken from Eq. (7). We always calculate P before θ so that this is an explicit method.

For simplicity, assume first that $b = 0$. In order to calculate θ, we take Eq. (21), substitute Eq. (7), and obtain

$$\theta_t = \frac{\epsilon^2}{P^6}\theta_{\alpha\alpha\alpha\alpha\alpha\alpha} + N(\alpha), \tag{25}$$

where $N(\alpha)$ consists of all the remaining terms after the highest order term, the sixth order term, is extracted. Taking the Fourier transform of Eq. (25) we get

$$\hat{\theta}_t(j) = -\epsilon^2\left(\frac{2\pi j}{P}\right)^6 \hat{\theta}(j) + \hat{N}(j), \tag{26}$$

where j is the wave number. This equation is solved using a Crank-Nicholson-like method

$$\frac{\hat{\theta}^{n+1}(j) - \hat{\theta}^n(j)}{\Delta t} = -\epsilon^2(2\pi j)^6\left(\frac{\hat{\theta}^{n+1}(j)}{2(P^{n+1})^6} + \frac{\hat{\theta}^n(j)}{2(P^n)^6}\right) + \hat{N}^n(j). \tag{27}$$

Since P^n and P^{n+1} are known, this is an explicit method for $\hat{\theta}^{n+1}(j)$.

If $b > 0$, then the velocity from Eq. (7) is found by taking the Fourier transform. In this case, the equation for $\hat{\theta}_t$ takes the form

$$\hat{\theta}_t(j) = \frac{-\epsilon^2(2\pi j/P)^6\hat{\theta}(j) + \hat{N}(j)}{1 + kb + b(2\pi j/P)^2}, \tag{28}$$

and a discretization analogous to Eq. (27) is used.

IV. SIMULATION RESULTS

In all the simulations presented below, we take $a = 0.1$ and $\epsilon = 0.005$. We vary c, k, and b. The results are qualitatively similar to those obtained using other choices of $a(>1/15)$ and ϵ.

A. Driven anisotropic surface diffusion

We begin by investigating the evolution of an interface governed by surface diffusion with deposition. Taking Eq. (14) with $k = b = 0$ we find the normal velocity to be

$$V = -\left[\frac{\delta E}{\delta \Gamma}\right]_{ss} + c(1 - \cos\theta). \tag{29}$$

The shape of the interface as it evolves is shown in Figs. 1 and 2. We are particularly interested in the coarsening behavior over time for the evolving interface. Figure 3 shows the horizontal positions of the kinks (red) and antikinks (blue) as the interface evolves. The coarsening is determined largely by the value of the driving force constant c. For smaller values of c, as in Figs. 3(a) and 3(b), we see an increased amount of coarsening resulting in fewer kinks and antikinks in the equilibrium shape. As c increases, there is a steady increase in the number of kinks and antikinks that remain as steady periodic structures are formed. We also see that the characteristic kink-ternary coarsening events take place. As c increases, the periodic structures begin to fluctuate with random occurrences of facet formation as shown in Fig. 3(e). At large values of c, the evolution exhibits chaotic behavior [Fig. 3(f)]. These results are consistent with those found earlier by Haußer and Voigt (see Fig. 16 in [22]).

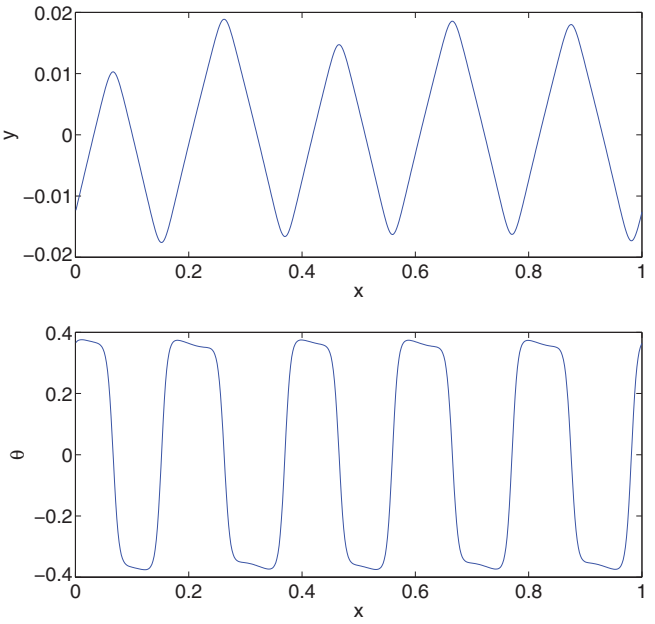

FIG. 2. (Color online) Interface and angle at time $t = 2.0 \times 10^{-4}$, a relatively late time in the evolution of the interface. The parameters are the same as in Fig. 1.

Figure 4 shows the coarsening rates of the evolving interface for different values of the driving force constant. We denote $\langle L\rangle$ to be the average kink-kink distance at any time with results taken as the average of ten different simulations. Although the range over which $\langle L\rangle$ varies is rather limited, we can identify three stages of coarsening as the evolution progresses. The first stage consists of fast amplitude growth with little coarsening as hill-valley structures emerge. The wave number of the interface in this initial stage is consistent with that predicted by the linear stability analysis, $j \approx 100/(\sqrt{3}\,\pi)$. The second stage is characterized by little amplitude growth, but fast power-law coarsening with $\langle L\rangle \sim t^{1/2}$. In the last stage we see little or no coarsening as an equilibriumlike state is reached. As the deposition c increases, we see that the fast-coarsening stage starts and ends at earlier times. Also, there are more kinks and antikinks, less total coarsening, in the final stage with increased values of c. These results are consistent with the nonchaotic regimes.

As shown in the Appendix, where a long-wave approximation of Eq. (14) is derived, the special case with with $k = b = 0$ is a higher-order convective Cahn-Hilliard equation of the form

$$q_t = [\epsilon^2 q_{xx} + q - q^3]_{xxxx} + \hat{c}qq_x, \tag{30}$$

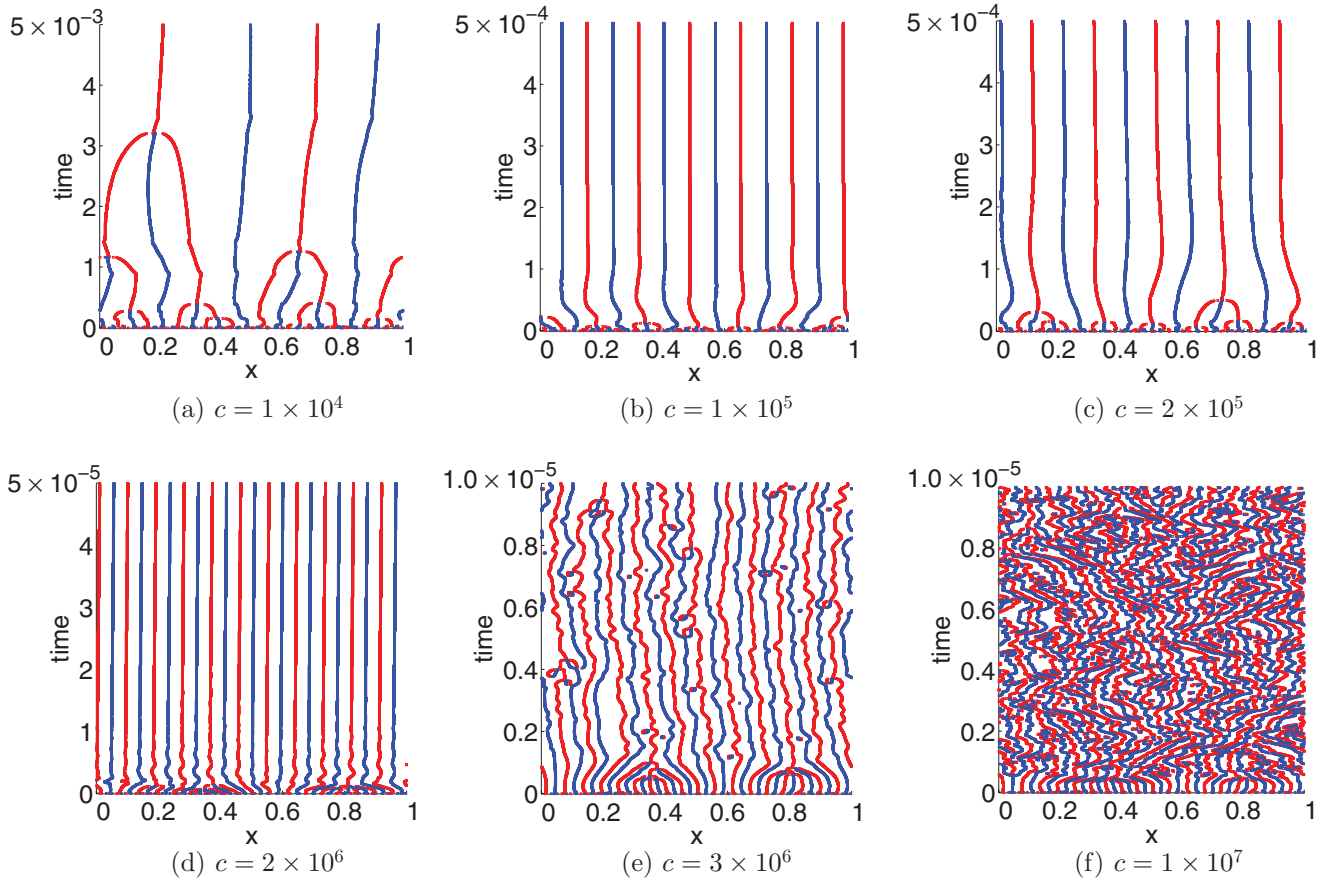

FIG. 3. (Color online) Space-time plots of kink [red (black)] and antikink [blue (gray)] positions during interface evolution governed by Eq. (14). There is no attachment-detachment or interface kinetics $k = b = 0$.

where q represents the slope of the interface and $\hat{c}$ is a constant related closely to our driving force constant c. A detailed analysis of this equation is found in Ref. [19]. Savina *et al.* describe the same driving force-dependent regimes for Eq. (30)

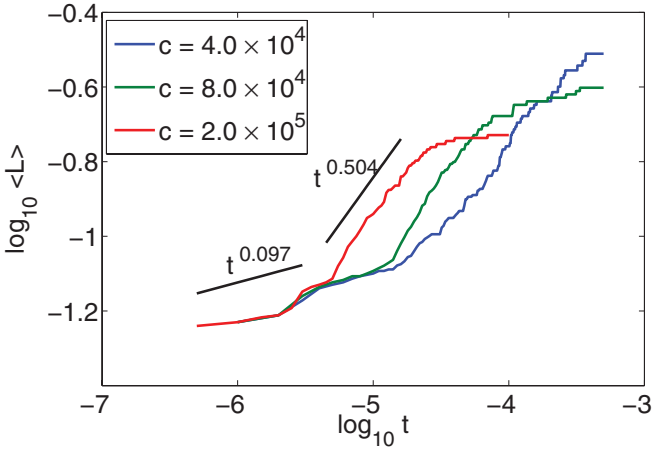

FIG. 4. (Color online) Coarsening dynamics for various values of c, the driving force constant. $\langle L \rangle$ is the average kink-kink distance at a given time with results taken as the average over ten simulations. The parameters are the same as in Fig. 3, with the values of c as labeled.

that we have found for the full geometric equation. They also show that for the nonchaotic regimes there are three stages of evolution, which are the same as those found here including the $t^{1/2}$ power-law coarsening in the fast-coarsening stage. By using the full geometric evolution equation in our analysis, we demonstrate that these results hold in a range beyond that for which the long-wave asymptotic theory applies.

B. Attachment-detachment

Next, we include a term modeling attachment-detachment dynamics, which accounts for the effects of evaporation and condensation. The normal velocity is

$$V = -\left[\frac{\delta E}{\delta \Gamma}\right]_{ss} + k\frac{\delta E}{\delta \Gamma} + c(1 - \cos\theta). \tag{31}$$

In Fig. 5 we show simulations in which we hold the deposition rate c fixed and allow k to vary. The results indicate a variable amount of coarsening depending on k. Specifically, increasing k leads to an increase in the amount of coarsening seen in the final interface shape. Indeed it is possible to have a value of k such that the equilibrium shape will contain one kink and one antikink. These results show that the amount of coarsening, and the time over which coarsening occurs, can be controlled by k.

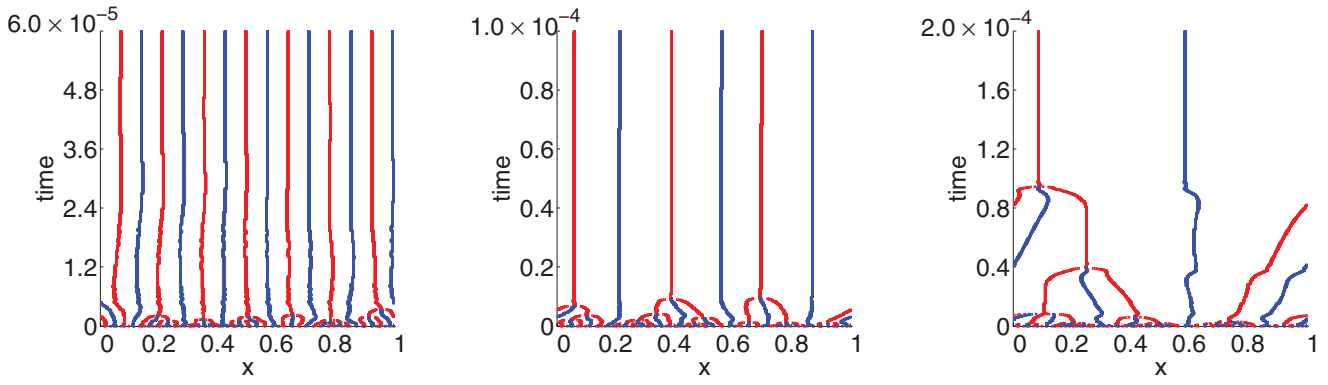

(a) $k = 4 \times 10^3$ (b) $k = 10^4$ (c) $k = 2 \times 10^4$

FIG. 5. (Color online) Space-time plots of kink [red (black)] and antikink [blue (gray)] positions during interface evolution in which surface diffusion is combined with attachment-detachment k as labeled and deposition $c = 8 \times 10^5$; there is no interface kinetics $b = 0$. The total amount of coarsening that takes place is determined by k.

Figure 6 shows the corresponding coarsening dynamics for various values of k. As before, $\langle L \rangle$ is the average distance between kinks, and this figure shows how $\langle L \rangle$ changes with time as the interface evolves. The results from ten different simulations are averaged. When $k = 0$, the evolution consists of the stages described previously in Fig. 4. When attachment-detachment is included, we identify four stages of evolution: one with little coarsening but fast amplitude growth, a stage of fast power-law coarsening, a stage of slow power-law coarsening, and finally no coarsening. In the fast and slow coarsening stages, a power law $\langle L \rangle \sim t^{\alpha}$ is obtained, where α is an increasing function of k. For example, when $k = 1.2 \times 10^4$, the fast power-law stage is given by $\langle L \rangle \sim t^{0.825}$ while the slow power-law stage is $\langle L \rangle \sim t^{0.327}$. In contrast, when $k = 0$, the fast power-law stage is given by $\langle L \rangle \sim t^{0.5}$. The attachment-detachment continues to cause coarsening after the fast coarsening stage, albeit at a slower rate as there is competition with the periodic structures that occur with surface diffusion alone. For larger values of k, the slow coarsening stage is extended in time, as is the amount of coarsening, so that fewer kinks and antikinks remain in the equilibrium state.

C. Interface kinetics

We next include a component representing the kinetic effects of the rearrangement of particles on the interface. As shown in Ref. [23], the effect of interface kinetics on an evolution driven primarily by surface diffusion is that there is a significant slowdown of the dynamics. Stöcker and Voigt previously studied an equation of the form

$$V - bV_{ss} = -\left[\frac{\delta E}{\delta \Gamma}\right]_{ss}, \tag{32}$$

where deposition and attachment-detachment are not considered. We extend their results by including these additional effects. The combination of interface kinetics and the driven anisotropic surface diffusion produces an interesting effect on the coarsening dynamics. The normal velocity is given by

$$V - bV_{ss} = -\left[\frac{\delta E}{\delta \Gamma} - bc\cos\theta\right]_{ss} + c(1 - \cos\theta). \tag{33}$$

We show how the inclusion of kinetic effects changes the deposition rates by which the three coarsening regimes are determined. We use $k = 0$ and $b = 0.01$. In particular, the value of the constant c needed to produce a particular regime is decreased significantly. Compare Fig. 3 with Fig. 7 and notice the change in the value of c for each regime. We observe that the effect of the kinetic term is to slow down the underlying dynamics of the evolving interface by slowing down the attachment and rearrangement of mass on the interface. Thus the deposition can more easily overwhelm the rearrangement of matter by surface diffusion, and so the chaotic and periodic regimes occur at much smaller deposition rates. Consequently, the interface dynamics resulting from deposition are strongly influenced by interface kinetics.

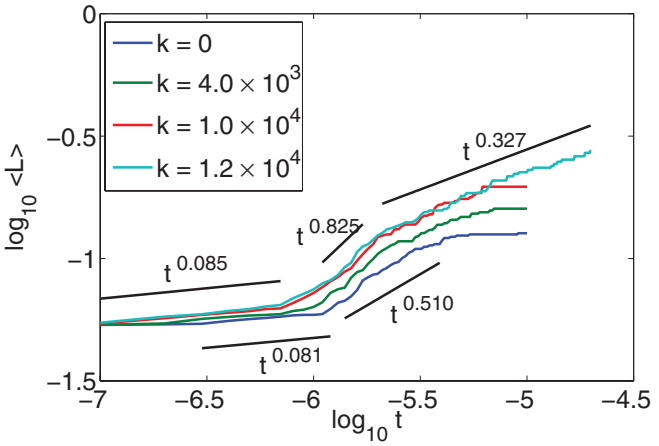

FIG. 6. (Color online) Coarsening dynamics for cases shown in Fig. 5 with the attachment-detachment coefficient k as labeled. $\langle L \rangle$ is the average kink-kink distance at a given time with results taken as the average over ten simulations.

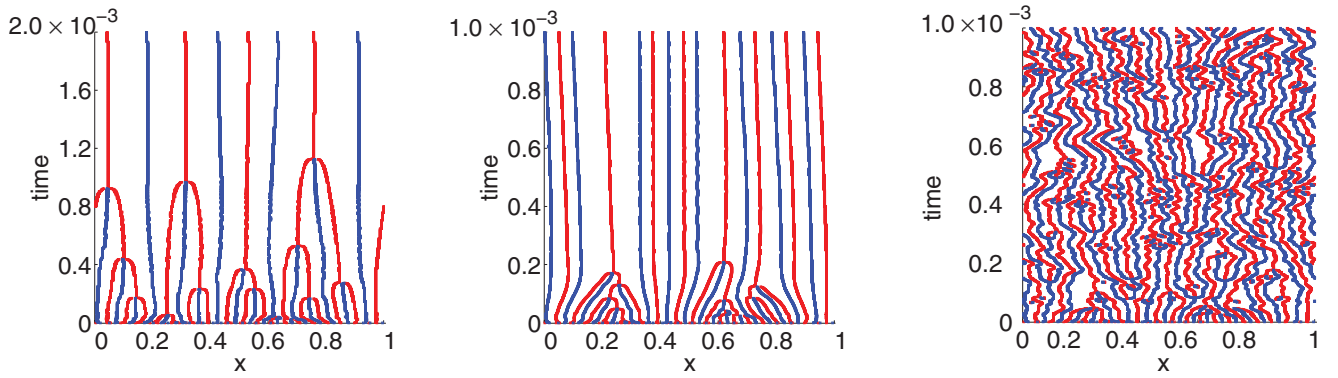

(a) $c = 8 \times 10^3$ (b) $c = 2 \times 10^4$ (c) $c = 8 \times 10^4$

FIG. 7. (Color online) Space-time plots of kink [red (black)] and antikink [blue (gray)] positions during driven anisotropic surface diffusion with interface kinetics $b = 10^{-2}$ and deposition c as labeled. There is no attachment-detachment $k = 0$. With interface kinetics the values of c needed to produce nonchaotic coarsening behavior are reduced.

In Fig. 8 we show a comparison between the coarsening dynamics of two evolving interfaces. In one case we have $c = 8.0 \times 10^4$ and $b = 0$, an interface evolving without consideration of kinetic effects. In the second case, we have $c = 4.0 \times 10^3$ and $b = 10^{-2}$ as an example of an interface evolving with kinetic effects. We have purposefully decreased the value of c in the second example in order to compare two examples from similar coarsening regimes. Both cases stop coarsening with approximately the same number of kinks and antikinks and both examples also exhibit a power-law coarsening similar to what has been observed previously in the fast-coarsening stage. The difference is in the time scale. The time when the fast-coarsening stage starts and ends is significantly increased in the case where interface kinetics is considered.

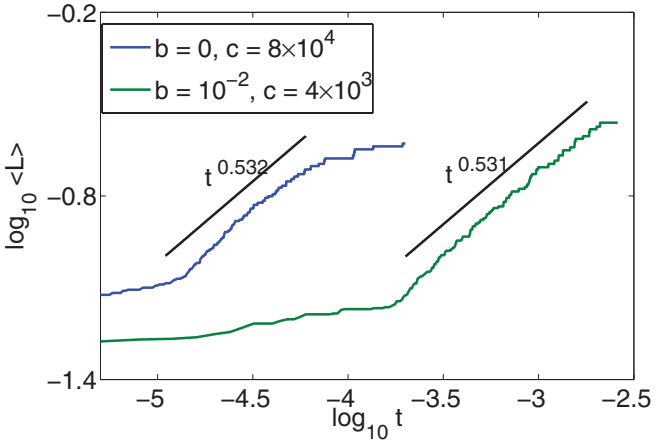

FIG. 8. (Color online) Coarsening dynamics for an interface evolving with kinetic effects considered ($b = 10^{-2}$) and one without kinetic effects ($b = 0$). In both cases, there is no attachment-detachment $k = 0$; see text for additional details. $\langle L \rangle$ is the average kink-kink distance at a given time with results taken as the average over five simulations.

D. All transport mechanisms

Finally, we discuss the inclusion of all of the transport mechanisms discussed in this paper. The normal velocity is

$$(1 + kb)V - bV_{ss} = -\left[\frac{\delta E}{\delta \Gamma} - \frac{bc}{1 + kb}\cos\theta\right]_{ss} + k\frac{\delta E}{\delta \Gamma} + c(1 - \cos\theta). \quad (34)$$

We have shown previously that attachment-detachment causes additional coarsening and that kinetic effects slow down the interface evolution. Therefore, given an interface whose dynamics are influenced by interface kinetics, we can add an attachment-detachment term to increase the total amount of coarsening that takes place leading to the equilibrium shape. The results are shown in Fig. 9 where we see that by increasing k, the amount of coarsening is increased as is the length of time during which coarsening occurs.

In Fig. 10 the corresponding average kink-kink distance is plotted as a function of time for driven anisotropic surface diffusion with parameters from Fig. 9, and k as labeled. For $k = 250$, there is a power-law coarsening rate of about $\langle L \rangle \sim t^{1/2}$ (not shown). However, for $k = 70$ we see the trend toward the four different coarsening stages: little coarsening, fast power-law coarsening with $\langle L \rangle \sim t^{0.672}$, slow power-law coarsening with $\langle L \rangle \sim t^{0.245}$, and then no coarsening.

V. CONCLUSION

We have considered the coarsening dynamics of a geometric evolution equation for driven anisotropic surface diffusion of a one-dimensional interface. We incorporated attachment-detachment, deposition, and kinetic effects from the rearrangement of atoms on the interface. The observed morphology consists of facets of constant slope separated by narrow transition intervals: the kinks and antikinks. As coarsening occurred, we showed in our numerical results that the only possible coalescence event is the kink-ternary one, where two kinks meet and annihilate an antikink.

We also presented simulation results for a variety of factors. We conclude that it is possible to control the amount of

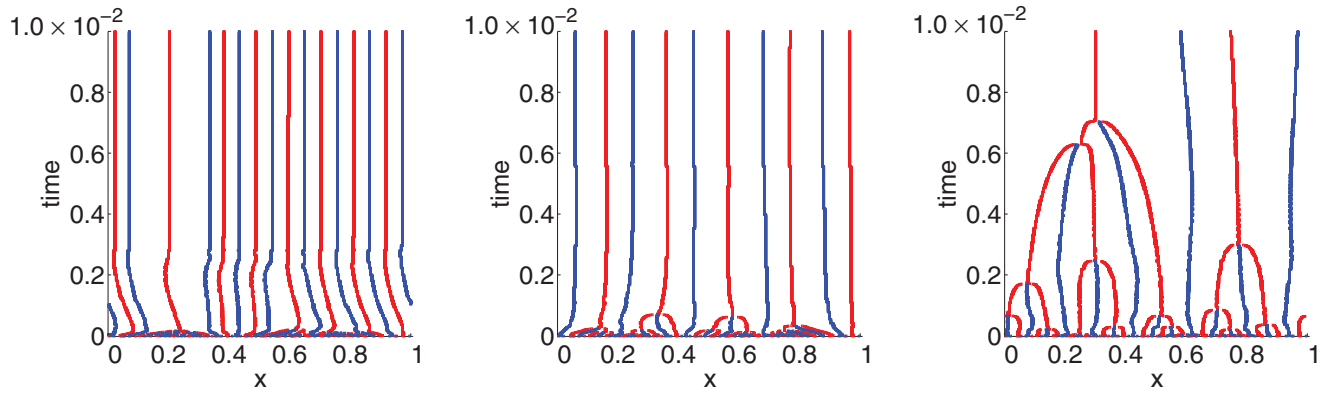

(a) $k = 0$ (b) $k = 100$ (c) $k = 1000$

FIG. 9. (Color online) Space-time plots of kink [red (black)] and antikink [blue (gray)] positions during driven surface diffusion with attachment-detachment, kinetic effects, and deposition. The total amount of coarsening that takes place is determined by k, the attachment-detachment coefficient. The inclusion of interface kinetics still causes a general slowdown in the overall dynamics. Here, $b = 10^{-2}$ and $c = 2 \times 10^4$, and k is as labeled.

coarsening during the dynamics by modifying the attachment rate. We also identified four stages of coarsening that occurred in the presence of attachment-detachment. Compared to the case with surface diffusion alone, attachment-detachment increases the amount and the time over which coarsening occurs. Specifically, the attachment-detachment term continues to drive coarsening for an extended period of time.

We also note that when kinetic effects are considered, the result is a significant slowing down of the dynamics of the interface evolution. As a result, the deposition rate to achieve a nonchaotic evolution regime must be significantly decreased. Thus when the dynamics of an interface which evolves under driven anisotropic surface diffusion are of interest, the kinetic effects caused by the rearrangement of particles on the interface should be considered.

Future work on this problem will involve the incorporation of elastic stress induced by misfit between the crystal lattices of the film and substrate. Preliminary work shows that elastic stress modifies the shape of the interface and introduces differences in the shapes of the kinks and antikinks [28]. This can modify coarsening rates [15]. In addition, we also plan to develop a model for surfaces that can incorporate the effects of attachment-detachment, deposition, interface kinetics, and elastic stress.

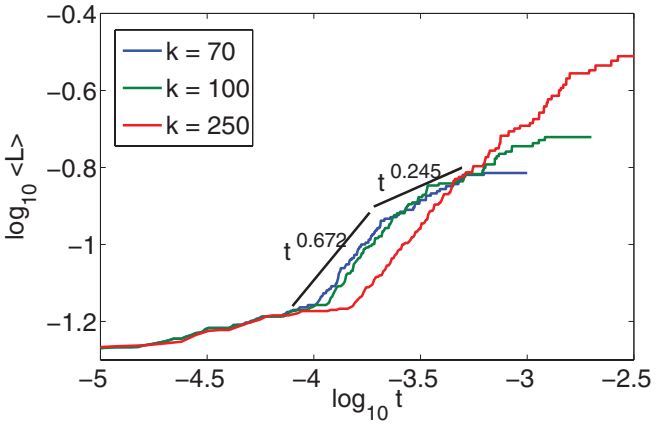

FIG. 10. (Color online) Coarsening dynamics for various values of k for the parameters from Fig. 9. $\langle L \rangle$ is the average kink-kink distance at a given time with results taken as the average over ten simulations.

ACKNOWLEDGMENTS

The authors thank Axel Voigt for stimulating discussions. The authors gratefully acknowledge partial funding from the National Science Foundation, Division of Mathematical Sciences.

APPENDIX: A HIGHER-ORDER CONVECTIVE CAHN-HILLIARD EQUATION

Here we derive a high-order convective Cahn-Hilliard equation using the long-wave approximation of Eq. (14),

$$(1 + kb)V - bV_{ss} = -\left[\frac{\delta E}{\delta \Gamma} - \frac{bc}{1+kb}\cos\theta\right]_{ss} + k\frac{\delta E}{\delta \Gamma} + c(1 - \cos\theta). \quad \text{(A1)}$$

The analysis follows very closely with that performed in Ref. [14], although in that case the attachment-detachment model is used. Here we use the full model associated with our work.

We consider a flat perturbed interface given by $y(x,t)$ where y is one-periodic in x, and we assume an expansion of the form $y(x,t) = \delta h(x,t) + O\left(\delta^2\right)$. Then we have

$$V = \delta h_t + O(\delta^2), \quad \text{(A2)}$$

$$V_{ss} = \delta h_{xxt} + O(\delta^2), \quad \text{(A3)}$$

$$\theta = \delta h_x + O(\delta^2), \quad \text{(A4)}$$

$$\kappa = \delta h_{xx} + O(\delta^2), \quad \text{(A5)}$$

$$\kappa_{ss} = \delta h_{xxxx} + O(\delta^2), \tag{A6}$$

$$\cos\theta = 1 - \tfrac{1}{2}\delta^2 h_x^2 + (\delta^3). \tag{A7}$$

We define τ in such a way that the stiffness function is given by

$$\tilde{\tau}(\theta) = 3\left(\frac{\theta}{\delta}\right)^2 - 1 =: \hat{\tau}\left(\frac{\theta}{\delta}\right), \tag{A8}$$

so that

$$\tilde{\tau}(\theta) = \hat{\tau}(h_x) + O(\delta). \tag{A9}$$

Finally we assume that c is related to δ as

$$c = \frac{\hat{c}}{\delta}, \tag{A10}$$

for some constant $\hat{c}$. Combining terms of order δ from Eq. (A1) gives

$$\begin{aligned}(1+kb)h_t - bh_{xxt} &= -\left(\hat{\tau}(h_x)h_{xx} - \epsilon^2 h_{xxxx} + \frac{b\hat{c}}{2(1+kb)}h_x^2\right)_{xx} \\ &\quad + k([\hat{\tau}(h_x)h_{xx} - \epsilon^2 h_{xxxx}] + \frac{\hat{c}}{2}h_x^2,\end{aligned} \tag{A11}$$

and differentiating both sides with respect to x and letting $q = h_x$ results in

$$\begin{aligned}(1+kb)q_t - bq_{xxt} &= -[\hat{\tau}(q)q_x - \epsilon^2 q_{xxx}]_{xxx} - \frac{b\hat{c}}{1+kb}(qq_x)_{xx} \\ &\quad + k[\hat{\tau}(q)q_x - \epsilon^2 q_{xxx}]_x + \hat{c}qq_x.\end{aligned} \tag{A12}$$

This equation can be written as

$$\begin{aligned}(1+kb)q_t - bq_{xxt} &= -[W'(q) - \epsilon^2 q_{xx}]_{xxxx} - \frac{b\hat{c}}{1+kb}(qq_x)_{xx} \\ &\quad + k[W'(q) - \epsilon^2 q_{xx}]_{xx} + \hat{c}qq_x,\end{aligned} \tag{A13}$$

where $W''(q) = \hat{\tau}(q)$. We have $W'(q) = q^3 - q$, so we obtain

$$\begin{aligned}(1+kb)q_t - bq_{xxt} &= (\epsilon^2 q_{xx} + q - q^3)_{xxxx} - \frac{b\hat{c}}{1+kb}(qq_x)_{xx} \\ &\quad - k(\epsilon^2 q_{xx} + q - q^3)_{xx} + \hat{c}qq_x.\end{aligned} \tag{A14}$$

When $k = b = 0$ this is a higher-order cCH equation associated with surface diffusion,

$$q_t = (\epsilon^2 q_{xx} + q - q^3)_{xxxx} + \hat{c}qq_x. \tag{A15}$$

This is precisely the equation which is considered in Ref. [19]. Results for the cCH equation are qualitatively similar to those obtained by the geometric evolution equation.

[1] D. J. Eaglesham and M. Cerullo, Phys. Rev. Lett. **64**, 1943 (1990).

[2] P. M. Petroff, in *Single Quantum Dots: Fundamentals, Applications, and New Concepts*, Topics in Applied Physics No. 90, edited by P. Michler (Springer-Verlag, Berlin, 2003), pp. 1–24.

[3] C. Misbah, O. Pierre-Louis, and Y. Saito, Rev. Mod. Phys. **82**, 981 (2010).

[4] G. Wulff, Z. Kristallogr. **34**, 449 (1901).

[5] W. K. Burton, N. Cabrera, and F. C. Frank, Philos. Trans. R. Soc. London, Ser. A **243**, 299 (1951).

[6] A. DiCarlo, M. E. Gurtin, and P. Podio-Guidugli, SIAM J. Appl. Math. **52**, 1111 (1992).

[7] B. J. Spencer, Phys. Rev. E **69**, 011603 (2004).

[8] J. J. Eggleston, G. B. McFadden, and P. W. Voorhees, Physica D **150**, 91 (2001).

[9] M. Ozdemir and A. Zangwill, Phys. Rev. B **45**, 3718 (1992).

[10] H. P. Bonzel and W. W. Mullins, Surf. Sci. **350**, 285 (1996).

[11] P. Politi and J. Villain, Phys. Rev. B **54**, 5114 (1996).

[12] N. Israeli and D. Kandel, Phys. Rev. B **62**, 13707 (2000).

[13] N. Israeli and D. Kandel, Phys. Rev. Lett. **88**, 116103 (2002).

[14] S. J. Watson, in *Free Boundary Problems: Theory and Applications*, International Series of Numerical Mathematics No. 147, edited by P. Colli, C. Verdi, and A. Visintin (Birkhauser Verlag, Basel/Switzerland, 2004), pp. 329–341.

[15] S. J. Watson, F. Otto, B. Y. Rubinstein, and S. H. Davis, Physica D **178**, 127 (2003).

[16] S. Watson (unpublished).

[17] J. Stewart and N. Goldenfeld, Phys. Rev. A **46**, 6505 (1992).

[18] F. Liu and H. Metiu, Phys. Rev. B **48**, 5808 (1993).

[19] T. V. Savina, A. A. Golovin, S. H. Davis, A. A. Nepomnyashchy, and P. W. Voorhees, Phys. Rev. E **67**, 021606 (2003).

[20] F. Haußer and A. Voigt, J. Cryst. Growth **275**, e47 (2005).

[21] A. A. Golovin, A. A. Nepomnyashchy, S. H. Davis, and M. A. Zaks, Phys. Rev. Lett. **86**, 1550 (2001).

[22] B. Li, J. Lowengrub, A. Rätz, and A. Voigt, Commun. Comput. Phys. **6**, 433 (2009).

[23] C. Stöcker and A. Voigt, J. Cryst. Growth **303**, 90 (2007).

[24] C. Herring, Phys. Rev. **82**, 87 (1951).

[25] J. W. Cahn and J. E. Taylor, Acta Metall. Mater. **42**, 1045 (1994).

[26] O. Pierre-Louis, Phys. Rev. Lett. **87**, 106104 (2001).

[27] T. Y. Hou, J. S. Lowengrub, and M. J. Shelley, J. Comput. Phys. **144**, 312 (1994).

[28] S. Torabi, S. Wise, S. Li, A. Voigt, J. Lowengrub, and P. Zhou, in *Simulations of Nonlinear Strongly Anisotropic, Misfitting Crystals and Thin Films*, MRS Symposia Proceedings No. 1087 (Materials Research Society, Pittsburgh, 2008), pp. V02–01.